Mechanical Systems and Signal Processing 250 (2026) 114168

Contents lists available at ScienceDirect

Mechanical Systems and Signal Processing

journal homepage: www.elsevier.com/locate/ymssp

Full length article

Effect of tracking resolution and loudspeaker arrangements on a headtracked active headrest noise control system

Chung Kwan Lai, Jordan Cheer *

Institute of Sound and Vibration Research, University of Southampton, University Rd, Southampton, SO17 1BJ, Hampshire, United Kingdom

ARTICLE INFO

Communicated by S. Marburg

Keywords:
Active headrest
Active noise control
Head-tracking

ABSTRACT

Head-tracking techniques offer the potential of improving the performance of local active noise control headrest systems during head movements. However, the effectiveness of head-tracked local active noise control can be limited by various aspects of the headrest design. This paper presents a thorough investigation into how head-tracking accuracy influences the control performance for both translational and yaw rotational head movements and, in addition, how this is affected by the geometry of the headrest control loudspeakers. The presented results highlight a notable difference in the attenuation performance achieved at the two ears when modelling errors exist between the physical plant response and the plant model utilised by the controller, which arise due to the accuracy of the head-tracking. It is demonstrated that the mismatch in performance between the two ears is influenced by the initial head position, the direction of head movements, and the layout of the headrest control loudspeakers. In the presence of plant modelling errors, the presented results reveal a trade-off between the balance in attenuation performance at the two ears and the spatial extent over which effective control is achieved. The presented insights can be utilised to help design local active noise control headrest systems with head-tracking that are well-suited to their intended application.

1. Introduction

Active headrest systems utilise the principle of local sound control [1] to create a localised zone of quiet around a listener's ears by driving secondary sources to appropriately interfere with a primary sound field [2,3]. While local control methods offer extended control at higher frequencies compared to global methods, which aim to control sound throughout an entire enclosed space [4], the control performance in practice is still limited at higher frequencies by the size of the zone of quiet which decreases with frequency. For instance, the diameter of the 10 dB zone of quiet, defined as the region within which at least 10 dB of noise attenuation is achieved, is approximately 1/10-th of the acoustic wavelength in a diffuse primary sound field [5]. This means that the microphones need to be placed close to the user's ear to increase the upper-frequency limit of control, which would restrict head movement and create potential user discomfort. Previous work has investigated overcoming these practical challenges by either shifting the zone of quiet from the physical microphone locations to virtual microphone positions using virtual sensing techniques [6–8], or by enlarging the zone of quiet through strategic error microphone placement and the use of additional secondary loudspeakers to enable minimisation of the particle velocity component in a direction perpendicular to the surface of the head [9]. Although these methods help ensure the ears remain within the zone of quiet, head movements can still degrade local control performance by shifting the ears outside of the quiet zone. Efforts have also been made to design an optimised plant model that maximises the

* Corresponding author.
E-mail address: J.Cheer@soton.ac.uk (J. Cheer).

https://doi.org/10.1016/j.ymssp.2026.114168
Received 7 November 2025; Received in revised form 12 March 2026; Accepted 15 March 2026

robust control performance during small head movements [10], but this approach does not ensure effective control performance over a large range of head movements.

To maintain control performance in the presence of significant head movements, considerable research interest has now focused on integrating head-tracking techniques into active headrest systems [11]. The principle of head-tracked local active noise control systems is to dynamically determine the current position, and potentially orientation [12], of the head using the headtracker and to correspondingly update the plant model utilised in the controller and the virtual sensing filter. This updating process can reduce the mismatch between the plant model used in the controller and the physical plant response and also allows the virtual microphone positions to be dynamically repositioned. This results in the zone of quiet dynamically following the head position and this has been shown to result in at least a 10 dB reduction in noise at frequencies up to at least 1 kHz in an anechoic environment [11] and has also been shown to offer significant benefits in practical environments, such as a car cabin [13].

The initial publications investigating head-tracked local active noise control discussed above [11,13] assumed perfect head-tracking, but in practice, some mismatch between the head-tracked position and the physical head position may arise and lead to errors between the plant model and the physical plant response, resulting in a degradation in the control performance. The issue of mismatch between the tracked and physical head positions may arise due to the absolute accuracy of the headtracker, the speed of the headtracker, or the spatial resolution for which the plant model has been measured during a calibration phase. Modern head-tracking systems generally provide high levels of accuracy, often exceeding the practical resolution limits of calibration grids [14] and the capability of head-tracking systems can be improved by utilising various vision algorithms, as recently discussed [12,15]. Therefore, the level of mismatch between the plant model used by the controller and the physical plant response in a head-tracked local active noise control system is predominantly governed by the spatial resolution for which the plant model is measured during the calibration phase. That is, the updated plant model is chosen solely from a predetermined set of models obtained during the calibration phase, or can be calculated by interpolating between these models [16,17]. Ideally, therefore, the plant responses would be measured across a very fine grid, giving a high spatial resolution and minimising the error between the physical and modelled plants. However, this would require a large set of plant models covering a large range of head positions, and potentially orientations, to be measured which may be infeasible for systems where the time and storage complexity of obtaining plant models is constrained. This consequently leads to a core design trade-off in a head-tracked active headrest system, namely between head-tracking accuracy and practical feasibility.

While it may be appropriate to consider active control systems that incorporate adaptive algorithms that can help maintain performance in the presence of plant modelling errors [18], as demonstrated in Ref. [19], the effectiveness of adaptive algorithms can still be limited by tracking resolution, potentially reducing convergence speed or even leading to instability. Nevertheless, it remains important to consider systems without adaptive control, as this helps identify the fundamental performance limitations of the system, particularly when the controller is sub-optimal. To gain understanding and physical insight into how the tracking resolution influences the realisable control performance and how this is also affected by the arrangement of the control loudspeakers, this paper presents a thorough investigation utilising a local active noise control headrest system. Building on a preliminary simulation-based study presented in Ref. [20], this paper presents the first systematic investigation into how different headrest loudspeaker spacings influence the performance of a multichannel feedforward local active control system equipped with head-tracking. The insight provided by this study provides new engineering knowledge that supports the design of local active noise control systems incorporating head-tracking.

In the first instance, in Section 2 the headtracker-equipped feedforward active noise control system is described, with both the control strategy and the physical headrest arrangement outlined. In order to understand how the tracking resolution requirements are influenced by the physical layout of the active headrest system, two headrest configurations are explored with different spacings between the two headrest loudspeakers. Since the loudspeaker spacing is often dictated by the physical design of the headrest system, it is important to understand how different headrest configurations influence system performance, as this can help identify design constraints and artefacts that may arise in practical implementations. Although previous work has explored the effect of the headrest loudspeaker positioning when utilising feedback control [3], which benefits from locating the loudspeakers as close as possible to the error microphones to minimise the group delay in the plant response, there has not been any explicit investigation presented when considering a multichannel head-tracked system utilising a feedforward control approach. Having introduced the headrest control systems, Section 3 examines the effect of both translational and rotational head movements on the plant responses for the two headrest configurations. Section 4 then presents an investigation into the impact of head-tracking resolution on control performance for both translational and rotational head movements for the two control loudspeaker configurations. Finally, Section 5 draws conclusions.

2. Headtracker-equipped multichannel active headrest system

In this section, the physical arrangement of the headtracker-equipped active headrest system is first described, before the multichannel feedforward control strategy is outlined. It is worth noting that the headrest configuration with the wider loudspeaker spacing presented in this paper is consistent with the setup utilised in previous work [19], whilst the second headrest configuration with the narrower loudspeaker spacing has not previously been reported.

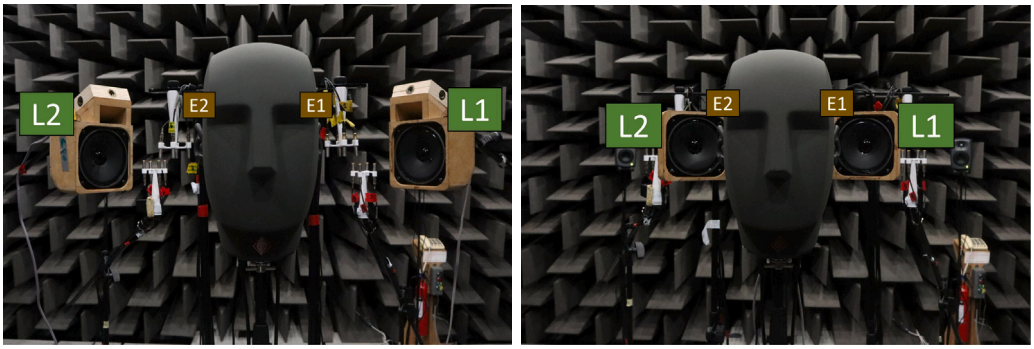

(a) (b)

Fig. 1. The front view of the (a): wide spacing and (b): narrow spacing configurations of the secondary loudspeakers (L1 and L2) in the active headrest placed inside an anechoic chamber, along with the error microphones in the ears of the dummy head (E1 and E2).

2.1. Physical setup of the headtracker-equipped active headrest

Fig. 1 shows the two different experimental realisations of the active headrest system positioned in an anechoic chamber. The first arrangement, shown in Fig. 1(a), illustrates the case where the two secondary loudspeakers, denoted as L1 and L2, are positioned 0.55 m apart (wide spacing); whilst the second arrangement, depicted in Fig. 1(b), represents the case where they are spaced 0.275 m apart (narrow spacing). These two headrest configurations have been selected as distinct cases that represent a feasible range of loudspeaker spacings for practical headrest systems. For example, while the narrow spacing may be consistent with practical designs intended for compact aircraft or automotive seating, the wide spacing may be more aligned with premium seating systems that can offer greater flexibility. The two cases considered here, therefore, enable a clear and systematic investigation of how loudspeaker spacing affects the performance of a head-tracked active headrest system without constraining the study to specific applications. Additionally, the loudspeakers are orientated at an angle of 65° and 30° for the wide and narrow-spaced configurations respectively, so that the drivers are directed towards the ears at the nominal head position of (0, 0) m. Both loudspeakers are used to minimise the pressures at the ears of the dummy head, as measured by the error microphones, E1 and E2, and the response between these loudspeakers and error microphones is referred to as the plant response. To ensure that the changes in the plant response are solely due to head movement and not influenced by room acoustics, the measurements for both configurations were taken in an anechoic chamber. The primary disturbance field is generated using 16 loudspeakers, which are evenly distributed around the head at equal angular intervals at a radial distance of 3 m, and assumed to be driven with uncorrelated random white noise. This ensures that the described power and cross spectral densities are time-invariant and allows the controller to be formulated in the frequency domain, as in Ref. [21]. Additionally, this approach allows the control performance to be assessed without any dependencies introduced by the directivity of the primary sound field, as reported in Ref. [22], and thus ensures the presented analysis is insightful for general noise control problems. The positions and rotational angles of the dummy head are controlled by a robotic positioning system to ensure both repeatability and precise alignment with the intended coordinates, thus allowing for accurate comparison between the two experimental arrangements. A series of sine-sweep measurements [23] have been conducted to obtain the primary and plant responses for each head position within a discrete translational grid of (0.4 m × 0.2 m), with a resolution of 2.5 cm, and a discrete rotational grid ranging from −27° to +27°, with a resolution of 9°, as illustrated in Fig. 2. To constrain the considered problem and focus on the head movements that are more common in an active headrest system, translational movement in the sway (left/right) and surge (front/back) directions, and rotational movement in the yaw directions, are considered in this work. Whilst movement in the other degrees of freedom, such as heave (up/down), pitch and roll, may become more relevant in specific applications, investigation of their influence on the headrest control performance has been left for future work.

2.2. Multichannel feedforward active control strategy

Fig. 3 shows the multichannel feedforward control system utilised to determine the control filters that drive the secondary loudspeakers to minimise the pressures measured at the error microphones. In order to focus on the physical limits of the control system rather than the controller itself, it has been assumed that the formulated controller is implicitly causal, as defined in Ref. [21], and that a perfect reference signal is available. This allows general insight to be provided that can be utilised to inform the design of practical controllers for various applications where both causality and coherence between the reference signals and error signals limit the achievable control performance.

The cost function minimised by the control system shown in Fig. 3 can be expressed in the frequency domain as the sum of the squared error signals given by

$$J = \mathbb{E}\left[\mathbf{e}^{\mathrm{H}}\mathbf{e} + \beta\mathbf{u}^{\mathrm{H}}\mathbf{u}\right] = \mathrm{tr}\left\{\mathbf{S}_{ee} + \beta\mathbf{S}_{uu}\right\}, \tag{1}$$

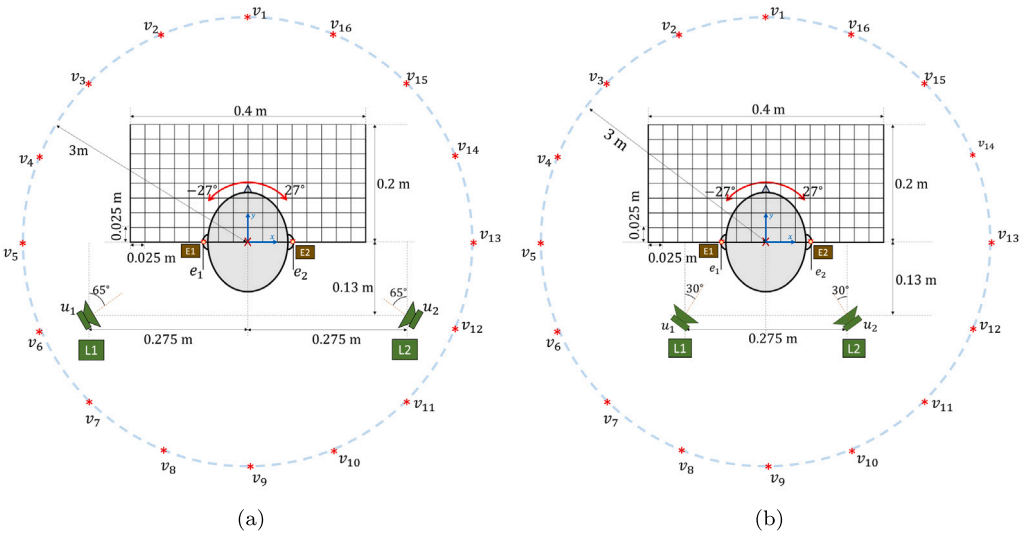

(a) (b)

Fig. 2. The geometry of the active headrest system under the (a): wide loudspeaker spacing and (b): narrow loudspeaker spacing configurations. Both configurations share the same head-tracking grid, where the head translates in the sway (left/right) and surge (front/back) translational directions over an area of 0.4 m × 0.2 m, and rotates within a yaw range of −27° to +27°. The minimum grid spacing for the translational grid is defined as 0.025 m, while the rotational grid uses 9°.

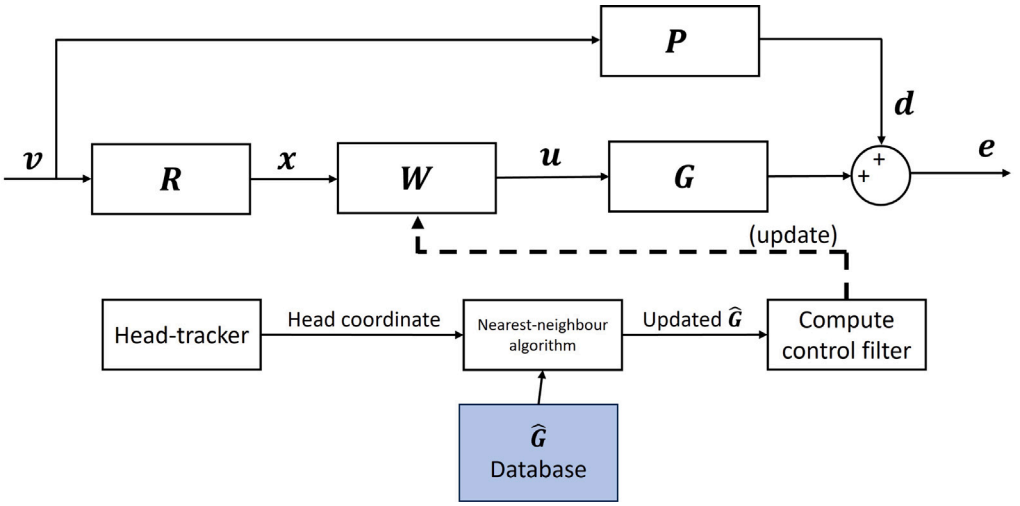

Fig. 3. The multichannel feedforward control system used for the headtracker equipped active headrest system.

where $\mathbf{e} = \begin{bmatrix} e_1 & e_2 \end{bmatrix}^{\mathrm{T}}$ denotes a complex vector of the two error signals measured at the ears; $\mathbf{u} = \begin{bmatrix} u_1 & u_2 \end{bmatrix}^{\mathrm{T}}$ denotes the vector of control signals used to drive the two secondary loudspeakers in the headrest; $\mathbb{E}[\cdot]$ denotes the expectation operator; $\mathrm{tr}\{\cdot\}$ denotes the trace operator; $\mathbf{S}_{ee}$ and $\mathbf{S}_{uu}$ are the spectral density matrices of the error signals and control signals, respectively, defined using the general notation of $\mathbf{S}_{mn} = \mathbb{E}\left[\mathbf{n}\mathbf{m}^{\mathrm{H}}\right]$ for any two complex vectors $\mathbf{m}$ and $\mathbf{n}$; $(\cdot)^{\mathrm{H}}$ denotes the Hermitian transpose; and $\beta = 1 \times 10^{-3}$ denotes the regularisation parameter. The value of β has been selected here to avoid very poor numerical conditioning with respect to inversion of the plant matrix, whilst avoiding tuning the regularisation to achieve enhancement in the control performance via an increase in the robustness to tracking uncertainty, as discussed in Ref. [17]. The vector of error signals can be expressed as

$$\mathbf{e} = \mathbf{d} + \mathbf{G}\mathbf{W}\mathbf{x}, \tag{2}$$

where $\mathbf{d} = \begin{bmatrix} d_1 & d_2 \end{bmatrix}^{\mathrm{T}}$ denotes the vector of disturbance signals measured by the error microphones at the ears, $\mathbf{x}$ is the complex vector of reference signals, $\mathbf{W}$ is a complex matrix of control filters between the reference signals and control signals, and $\mathbf{G}$ denotes the physical plant responses between the secondary loudspeakers and the error microphones. By substituting Eq. (2) into Eq. (1), Eq. (1) can be expressed in the Hermitian quadratic trace form. This allows the matrix of optimum control filters that minimise Eq. (1) to

be derived and expressed as [18]

$$\mathbf{W}_{opt} = -\left[\mathbf{G}^{\mathrm{H}}\mathbf{G} + \beta\mathbf{I}\right]^{-1}\mathbf{G}^{\mathrm{H}}\mathbf{S}_{xd}\mathbf{S}_{xx}^{-1}, \tag{3}$$

where $\mathbf{I}$ is an identity matrix; $\mathbf{S}_{xd} = \mathbf{P}\mathbf{S}_{vv}\mathbf{R}^{\mathrm{H}}$ is the spectral density matrix between disturbance and reference signals; $\mathbf{S}_{xx} = \mathbf{R}\mathbf{S}_{vv}\mathbf{R}^{\mathrm{H}}$ is the spectral density matrix of the reference signals; $\mathbf{P}$ denotes the matrix of primary paths from the 16 primary sources to the two error microphones at the ears; $\mathbf{S}_{vv}$ is the spectral density matrix corresponding to the complex source strengths of the primary sources, $\mathbf{v} = \begin{bmatrix} v_1 & v_2 & \cdots & v_{16} \end{bmatrix}^{\mathrm{T}}$; and $\mathbf{R} = \mathbf{I}$ is the response from the primary sources to the reference signals which reflects the assumption that the reference signals perfectly represent all primary sources. As the primary sources are defined as uncorrelated with equal source strength, $\mathbf{S}_{vv}$ is diagonal and is modelled here as an identity matrix. Since the described active headrest system is fully-determined (i.e. the number of secondary loudspeakers is equal to the number of error microphones), the cost function given by Eq. (1) will theoretically be 0 under optimal control, provided no regularisation parameter is introduced. Achieving this optimal condition, however, requires perfect prior knowledge of both the plant responses and the disturbance signals. In practice, a model of the plant response, $\hat{\mathbf{G}}$, would usually be obtained prior to the control stage to compute the controller, which implies that optimal attenuation can only be achieved for the case when a perfect plant model is available, i.e. $\hat{\mathbf{G}} = \mathbf{G}$. This is not practically feasible due to various factors, especially for the active headrest system, where the plant responses are sensitive to slight changes in head position. Similarly, in practice, the statistical properties of the primary disturbance $\mathbf{S}_{xd}$ would need to be estimated either by virtual sensing methods [8,21] or by direct measurement during the calibration stage. In this case, estimation errors may result due to both head movements and changes in the disturbance sound field, leading to degradations in the attenuation performance. Although the effect of both plant modelling errors and primary field estimation errors are important, more insight can be obtained by isolating the contribution of these two terms. Therefore, it is assumed in this work that the statistical properties related to the disturbance signals are perfectly known and the degradation in control performance is solely due to limitations in the plant model. For the case where the statistics of the disturbance sound field are perfectly known, but there is a mismatch between the physical and modelled plant responses, the controller is obtained by replacing $\mathbf{G}$ in Eq. (3) with $\hat{\mathbf{G}}$ to give

$$\mathbf{W}_{\mathrm{o}} = -\left[\hat{\mathbf{G}}^{\mathrm{H}}\hat{\mathbf{G}} + \beta\mathbf{I}\right]^{-1}\hat{\mathbf{G}}^{\mathrm{H}}\mathbf{S}_{xd}\mathbf{S}_{xx}^{-1}, \tag{4}$$

which results in a sub-optimal controller.

As discussed in the introduction, head-tracking can be incorporated into the active headrest system to enable the plant model, $\hat{\mathbf{G}}$, to be dynamically updated depending on the current head position and thus reduce the mismatch between the plant model and the physical plant response during control. Incorporation of head-tracking into an active headrest system can be split into two distinct stages. In the first, or calibration stage, a plant model, $\hat{\mathbf{G}}$, is measured for each head position and orientation as defined by the tracking grid shown in Fig. 2. Then, during the control stage, the headtracker detects the current head position and orientation, and updates $\hat{\mathbf{G}}$ accordingly when calculating the control filters, $\mathbf{W}$. If the head position and orientation correspond exactly to a point on the tracking grid, then, excluding all other sources of error and uncertainty, $\hat{\mathbf{G}} = \mathbf{G}$; however, if the physical head position detected by the headtracker during control does not exactly correspond to a point on the tracking grid, then the plant model may be set as either the plant response corresponding to the geometrically nearest tracking grid point, or an interpolated plant model may be used [16,17]. In this work, the nearest neighbour method, which updates $\hat{\mathbf{G}}$ to be equal to the model for the closest tracking grid point to the physical head position, is utilised; this avoids introducing the complexities associated with interpolation strategies and focuses this paper on the effects of tracking resolution directly. In this case, the error between the plant model and physical plant response can be simply reduced by increasing the resolution of the tracking grid. However, increasing the tracking resolution increases the time required for the calibration stage and the memory required to store the plant models covering a large set of head positions and orientations. Consequently, there will be a trade-off between the control performance and the head-tracking resolution.

To evaluate control performance, the spectral density matrix of the signals at the error microphones after control, $\mathbf{S}_{ee}$, can be obtained by substituting Eq. (4) into Eq. (2), to give

$$\begin{aligned}\mathbf{S}_{ee} =& \mathbf{S}_{dd} - \mathbf{S}_{dd}\hat{\mathbf{G}}\left(\hat{\mathbf{G}}^{\mathrm{H}}\hat{\mathbf{G}} + \beta\mathbf{I}\right)^{-1}\mathbf{G}^{\mathrm{H}} - \mathbf{G}\left(\hat{\mathbf{G}}^{\mathrm{H}}\hat{\mathbf{G}} + \beta\mathbf{I}\right)^{-1}\hat{\mathbf{G}}^{\mathrm{H}}\mathbf{S}_{dd} \\ &+ \mathbf{G}\left(\hat{\mathbf{G}}^{\mathrm{H}}\hat{\mathbf{G}} + \beta\mathbf{I}\right)^{-1}\hat{\mathbf{G}}^{\mathrm{H}}\mathbf{S}_{dd}\hat{\mathbf{G}}\left(\hat{\mathbf{G}}^{\mathrm{H}}\hat{\mathbf{G}} + \beta\mathbf{I}\right)^{-1}\mathbf{G}^{\mathrm{H}},\end{aligned} \tag{5}$$

where $\mathbf{S}_{dd}$ is the spectral density matrix of the disturbance signals which, following Fig. 3, can be expressed as $\mathbf{S}_{dd} = \mathbf{P}\mathbf{S}_{vv}\mathbf{P}^{\mathrm{H}}$. Since it is assumed here that the system is linear, the absolute level of the disturbance field is arbitrarily determined by the definition of $\mathbf{S}_{vv}$ as an identity matrix.

Following the definition of these spectral density matrices, the overall attenuation performance achieved by the headrest control system can be expressed in decibels as

$$L_e = -10\log_{10}\left|\frac{\mathrm{tr}\left\{\mathbf{S}_{ee}\right\}}{\mathrm{tr}\left\{\mathbf{S}_{dd}\right\}}\right|. \tag{6}$$

For active headrest systems, it may also be pertinent to consider the attenuation performance at the individual ears, which can be defined for the ith ear as

$$L_{e_i} = -10\log_{10}\left|\frac{S_{e_i e_i}}{S_{d_i d_i}}\right|. \tag{7}$$

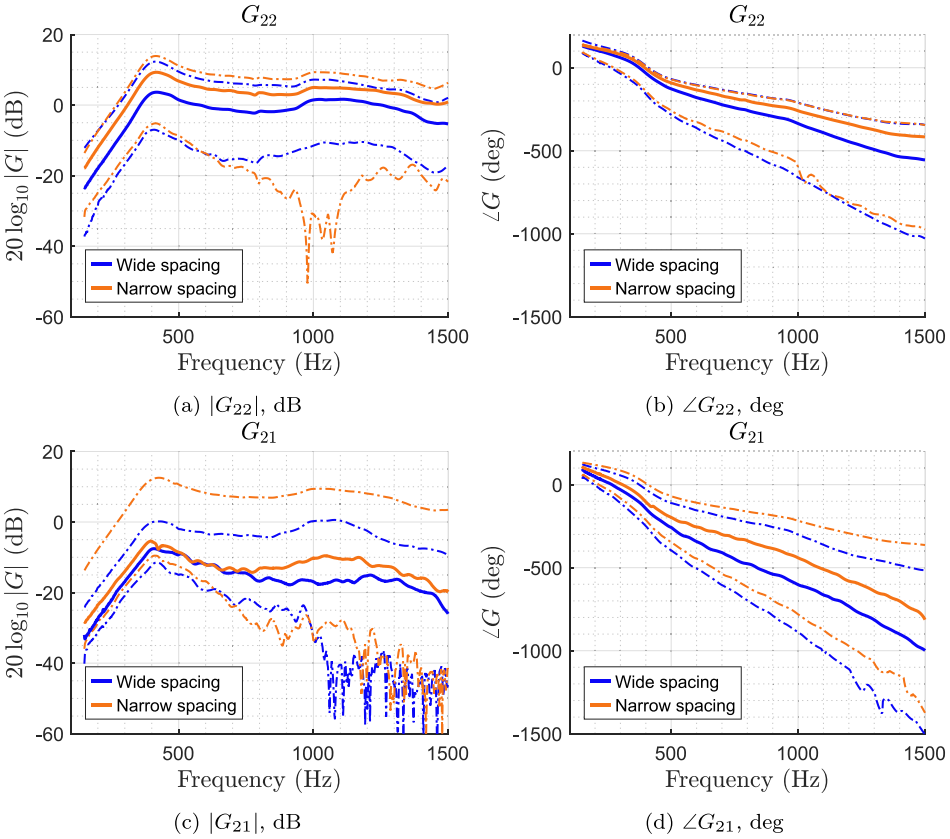

Fig. 4. The range of the plant responses between the right and left secondary loudspeakers (L2 and L1) and the right error sensor (E2) across all head positions and rotations for the wide and narrow loudspeaker spacing configurations. The solid lines represent the plant response at the head translational position of (0, 0) m with rotational angle of 0°, and the dashed–dotted lines represent the minimum and maximum bounds on the responses for all head positions and rotations described in the schematic diagram presented in Fig. 2.

For a real-time system, the performance according to Eq. (6) and Eq. (7) can be evaluated by measuring the pressures at the error microphones with and without control; however, in the present study the power spectral densities corresponding to the error and disturbance signals are calculated as laid out above using the measured system responses.

3. The effect of head movement on the plant response

This section presents an investigation into the effect of translational and rotational head movements on the plant responses for the two different headrest configurations, as described in Section 2.1 and shown in Fig. 1 and Fig. 2. Fig. 4 shows the plant responses measured between each headrest loudspeaker and the right ear for the two headrest configurations; in each plot the thick solid line shows the response measured at the nominal head position, with coordinates (0, 0) m and a rotational angle of 0°, and the dashed–dotted lines show the minimum and maximum bounds for the responses measured at all head positions and rotations.

It can be observed from the presented results that there are some general differences between the responses depending on the loudspeaker spacing. For the direct path, G_{22}, the responses for the widely spaced configuration, as shown in Fig. 4(a), exhibit a magnitude range of approximately ±10 dB, with a relatively consistent shape across frequency. In contrast, the results for the narrowly spaced configuration show a larger variation in level, especially at frequencies around 1 kHz where several dips in the minimum bound on the responses occur. These dips can be related to the near-field head shadowing effect, which occurs when the wavelength is comparable to the diameter of the dummy head and is particularly pronounced at certain head positions [24]. Additionally, the response at the nominal head position is about 5 dB higher than for the widely spaced case, since the loudspeakers are positioned closer to the ears. This is also reflected in the phase response, shown in Fig. 4(b), where the narrow spaced configuration exhibits a lower phase delay compared to the widely spaced configuration, owing to the reduced group delay. For the cross path, G_{21}, the magnitude range in the widely spaced configuration, as depicted in Fig. 4(c), starts at approximately ±10 dB at low frequencies but gradually increases with frequency, showing multiple dips at frequencies above 1 kHz where the near-field shadowing effect begins to occur. A similar behaviour is observed for the narrowly spaced loudspeaker configuration, although it exhibits a larger magnitude range across frequencies. The wider range observed in the narrow configuration mainly results from

the increase in the maximum bound on the magnitude response, which arises through the potentially small geometrical distance between each ear and the corresponding cross-path loudspeaker (right ear to left loudspeaker in the presented case) for certain head positions. In terms of the phase response for the cross-path at the nominal head position, as shown in Fig. 4(d), the trend is similar to that of the direct path, except that the narrowly spaced configuration exhibits a lower phase delay due to the reduced group delay between the secondary cross-path loudspeakers and the error microphone. This reduced group delay is consistent across all head positions and, therefore, while the range of phase responses is similar for the two configurations, the phase response for the narrowly spaced configuration remains consistently higher than that of the wide spacing setup.

4. The effect of tracking resolution on the control performance

This section presents an investigation into the effect of the tracking resolution on the control performance for the two active headrest configurations described in Section 2.1. Based on the plant response variations presented in Fig. 4 and discussed in Section 3 it is clear that the observed variations due to head translation and rotation in the active headrest system depend on the arrangement of the loudspeakers. While both configurations will benefit from the use of head-tracking to allow a reduction in the mismatch between the plant model $\hat{\mathbf{G}}$ used by the controller and the physical plant response $\mathbf{G}$, the controller may still be limited by the tracking resolution that arises from the calibration procedure. This section presents a study investigating how the performance of the active headrest system varies with tracking resolution and the type of head movements for the two different active headrest configurations; in particular, this study aims to address whether there are any differences in the tracking resolution requirements for the different headrest loudspeaker configurations.

4.1. The effect of head-tracking resolution on control performance

In a headtracker-equipped active headrest system, the geometrical errors between the physical head position and the head position assumed by the headtracker will lead to an error between the physical plant response $\mathbf{G}$, and the plant model, $\hat{\mathbf{G}}$, used in the controller. Fig. 5 illustrates the potential geometrical errors between the physical head position/rotation and the modelled head position/rotation, which will lead to errors between the physical plant response $\mathbf{G}$ and the plant model $\hat{\mathbf{G}}$. The pink cross/line in each case denotes the modelled head position/rotation, and the coloured arrows denote the physical head positions corresponding to three different levels of position/rotation error. These different levels of error correspond to the use of different grid resolutions in the formation of the plant model database. That is, for translations in the surge and sway directions, the blue arrows represent a grid resolution of 0.025 m, the green arrows represent a grid resolution of 0.05 m and the red arrows a grid resolution of 0.075 m; for rotations in yaw, the blue arrows represent a grid resolution of 9°, the green arrows a grid resolution of 18° and the red arrows a grid resolution of 27°.

It is important to note that the control performance depends on the initial position of the head and the direction of movement. Specifically, the degradation in the control performance when the head moves from an arbitrary position A to position B may not be the same as when movement occurs from position B to A. Therefore, it is necessary to consider all possible head movements within the tracking grid in different directions of head movement to understand the physical behaviour. However, as both arrangements for the active headrest from Fig. 2 are geometrically symmetric, the number of results presented in this study can be reduced. Specifically, only sway movements to the right direction, as shown in Fig. 5(a), are considered here, since sway movements to the left are geometrically symmetric and thus exhibit the same behaviour. Conversely, it is necessary to examine surge in the forward and backward directions separately, as shown in Fig. 5(b) and Fig. 5(c), since they influence the acoustic response differently. Finally, only clockwise yaw rotations are considered, as shown in Fig. 5(d), since the behaviour for anticlockwise rotations is equivalent.

To effectively capture the general effect that the tracking resolution has on the attenuation performance across the entire tracking grid, Fig. 6 shows the overall attenuation performance, computed according to Eq. (6), for various types of head movement, tracking resolution and loudspeaker configuration. The solid line plots represent the overall attenuation performance, calculated according to Eq. (6) for each combination of head movement within the tracking grid, averaged across all possible head movements, and the shaded regions indicate the range of attenuation performance across the same head movements. It can be seen from these results that for all head movements and loudspeaker configurations the attenuation performance decreases monotonically with frequency after a low-frequency threshold, below which a roll-off occurs. This roll-off can be related to the use of a constant regularisation parameter of $\beta = 1 \times 10^{-3}$ that constrains the control effort and limits the attenuation performance, particularly at lower frequencies where the plant response is lower, as shown in Fig. 4, and the condition number is generally higher. It can also be seen from these results that, for all head movements and loudspeaker configurations, as the tracking resolution becomes finer, the overall attenuation performance increases. However, as the resolution increases, the range of attenuation performance across all head positions increases for translational movements, but decreases slightly for rotational movements. It can also be observed from the results for both loudspeaker spacings that both the average and range of attenuation performance vary quite notably for the different types of head movement. For translational movements, it can be seen that sway movements are characterised by a larger range in the level of attenuation compared to both forward and backward surge for both loudspeaker spacings. Notably, as previously commented, it can also be seen that there is a difference in the level of performance between surge to the front and to the rear, with forward movements showing a smaller range of attenuation performance and providing a wider bandwidth over which the control attenuation exceeds 10 dB. For the considered rotational spacings, the range of performance tends to be larger than for the considered translational grids, although a direct comparison is somewhat limited. Finally, although the observed trends in attenuation performance are similar for the two loudspeaker spacings and the differences in the average performance are relatively small, it is clear from the

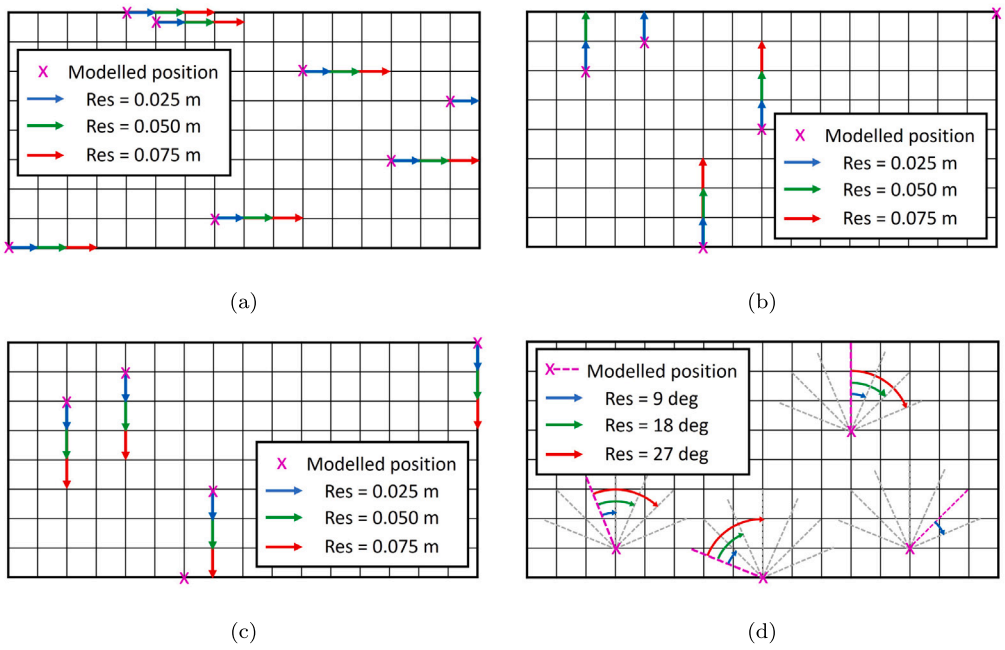

Fig. 5. The potential errors between the physical (denoted by the coloured arrows) and modelled (denoted by the pink cross/line) head positions in the (a): sway (right), (b): surge (front), (c): surge (back) and (d): yaw rotation (clockwise). The yaw rotation angle is assumed to be fixed at 0° for the translational cases.

results presented in Fig. 6(b) that the narrow loudspeaker spacing configuration shows a much larger range in the attenuation performance across all combinations of movements and tracking resolutions. This not only highlights a key limitation of using a spatially averaged attenuation as a performance metric, since it masks the greater spatial variability which is especially observed in the narrow loudspeaker spacing configuration, but also underscores how the overall effectiveness of the active headrest system is strongly dependent on the geometrical configuration of the loudspeakers.

Headtracker-equipped active headrest systems should ideally provide a high level of attenuation performance for all head positions and rotations. However, it has been shown from the results presented in Fig. 6 that the control performance for both loudspeaker configurations depends, to varying degrees, on the head position and rotation. To provide more insight into the range of performance, Fig. 7 shows the percentage of head movements, out of all possible head movements within the tracking grid for a given type of head movement and tracking resolution, that achieve an attenuation performance greater than 10 dB up to a considered frequency. The 10 dB attenuation level is chosen to align with the 10 dB zone of quiet definition used in the literature [1]. In each plot in Fig. 7, the overall attenuation performance, computed using Eq. (6), is represented by the solid lines, while the attenuation performance for the left and right error microphones, computed using Eq. (7), are depicted as dotted and dashed lines respectively. For both headrest configurations, a coarser tracking resolution results in a lower percentage value for all types of head movement, which aligns with the trends presented in Fig. 6. The results in the case of the wide loudspeaker spacing configuration, as depicted in Fig. 7(a), show a clear difference between the overall attenuation performance and the attenuation achieved at the individual microphones for all types of head movement and tracking resolutions. For example, in the case of sway movements with a tracking resolution of 0.025 m, the overall attenuation performance percentage drops from 100% to 0% between 560 Hz and 1060 Hz, while the percentage for the individual microphones does not reach 0% even at frequencies as high as 1500 Hz. The mismatch between the overall attenuation performance and that observed at the individual microphones is less pronounced in the results for the narrow loudspeaker spacing configuration, as shown in Fig. 7(b). It is also interesting to observe for the narrow loudspeaker spacing that in the case of sway movements with the finest tracking resolution, the overall percentage value does not reach 100% at low frequencies, which suggests quite limited attenuation performance for some head positions, but only decreases to 0% at 1400 Hz, which is a relatively high frequency compared to the wide loudspeaker spacing configuration; these observations are consistent with the large range of performance presented in Fig. 6(b) for the narrow loudspeaker spacing. These results highlight that, although the narrow spacing configuration achieves improved overall attenuation performance at higher frequencies for some sway movements compared to the wide loudspeaker spacing, the spatial consistency of the performance is limited at low frequencies, restricting the effective tracking range where attenuation performance remains reliably high. For surge movements in both directions and yaw rotations, the narrow spacing configuration does not extend the frequency at which the percentage drops to 0% compared to the wide loudspeaker spacing configuration and also fails to achieve 100% spatial coverage at low frequencies. For these specific types of head movements, no clear advantage over the wider loudspeaker configuration is observed in terms of overall attenuation when assessed using the percentage-based evaluation shown in Fig. 6.

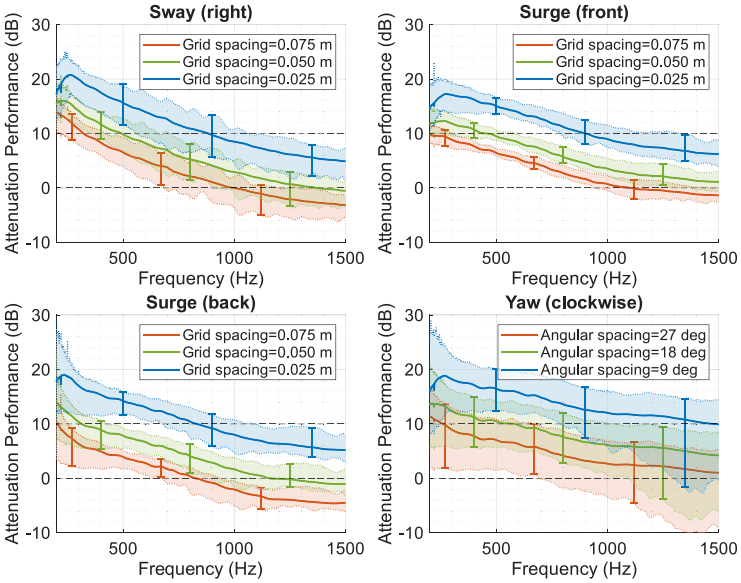

(a)

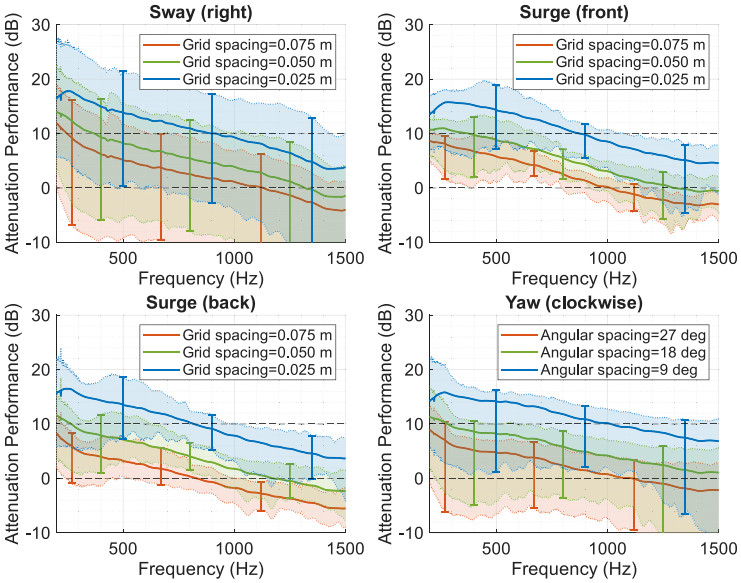

(b)

Fig. 6. The overall attenuation performance computed from Eq. (6) plotted against frequency when the head undergoes different types of movements for the (a): wide spacing arrangement and (b): narrow spacing arrangement. The line plots represent the overall attenuation performance averaged across all head movements, and the shaded regions represent the range of attenuation performance for all head movements.

4.2. The effect of initial head position on head-tracked control performance

While the percentage plots in Fig. 7 highlight a potential discrepancy between the attenuation performance measured for individual microphones and the overall system, they do not provide information about the specific head positions where high attenuation performance is maintained during head movements. To further understand the spatial dependence of the attenuation performance for the different head movements and loudspeaker configurations, it is useful to examine the frequencies for which the attenuation performance level first crosses below 10 dB for each head position. Fig. 8 and Fig. 9 show colour maps presenting the frequency at which the attenuation level, evaluated for the overall system (according to Eq. (6)) and the individual error microphones (according to Eq. (7)), first crosses below 10 dB for each initial head position. These maps, generated for the finest resolution grid, cover each initial head position and translational head movement described in Fig. 5 and correspond to the wide and narrow

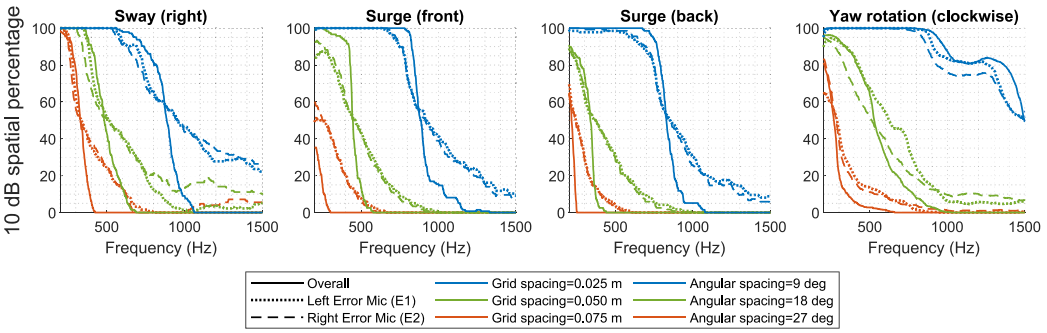

(a) Wide spacing configuration.

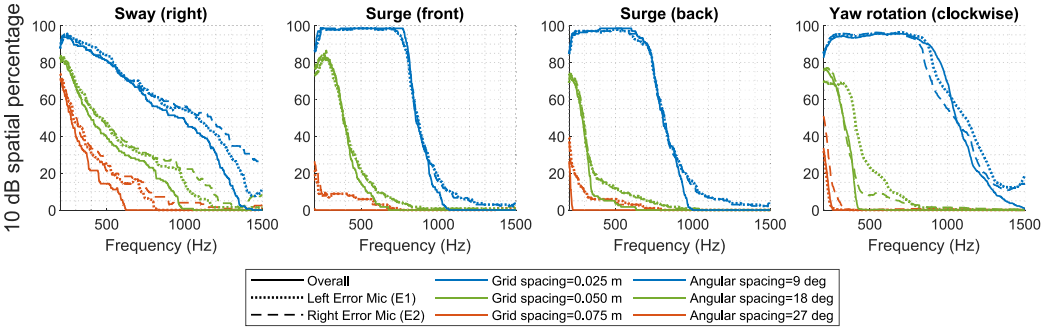

(b) Narrow spacing configuration.

Fig. 7. The percentage among all head movements for the (a): wide spacing configuration and (b): narrow spacing configuration for different tracking resolution and types of head movement, having an attenuation performance level more than 10 dB.

loudspeaker spacing configurations, respectively. From Fig. 8 it can be seen that for the wide loudspeaker spacing configuration, all types of translational head movements exhibit a mismatch in the attenuation performance between the left and right error microphones. For example, in the case of sway movements, as shown in Fig. 8(a), the frequency at which the attenuation performance crosses below 10 dB exceeds 1500 Hz for the left error microphone in the region $-0.2 \leq x \leq -0.125$ m and decreases in the positive x-direction, while for the right error microphone this performance is achieved in the region $0.075 \leq x \leq 0.2$ m and decreases in the negative x-direction. This behaviour can be related to the relative geometrical positions of the secondary loudspeaker and the error microphone in each direct path, as the change in magnitude and phase for sway movements, which closely relate to the changes in the straight-line distance between the loudspeaker and the error microphone, are smaller for head positions closer to the x-coordinate of the secondary loudspeakers. Moreover, the corresponding changes in the straight-line distance differ between the left and right direct paths, depending on the initial head position, which results in a highly asymmetric variation in the straight-line distance between the two paths and, consequently, a greater imbalance in performance between the ears. The colour maps for the overall attenuation performance, however, show a maximum frequency of 1 kHz at $x = -0.025$ m, with a decrease in both the positive and negative x-directions, since the performance in this case, given by Eq. (6), includes the average of the squared error signals at both the left and right error microphones. Similar observations regarding the spatial discrepancy between the left and right error microphones can also be seen for surge movements, as shown in Fig. 8(b) and Fig. 8(c). However, in this case, the region where the 10 dB crossing frequency exceeds 1500 Hz appears at the grid coordinates (0, 0.2) m for the left error microphone and (0, −0.2) m for the right error microphone; this frequency then decreases in the direction diagonally upwards in the left and right directions, for the left and right error microphones respectively. An additional spatial feature can also be observed in the backward surge case, where a region with a 10 dB crossing frequency below 200 Hz occurs at grid coordinates (−0.175, 0.025) m and (0.175, 0.025) m for the left and right microphones, respectively. This indicates that at these locations the control attenuation is below 10 dB at 200 Hz and this behaviour is also reflected in Fig. 7(a), where the percentage for the left and right error microphones is below 100% across all frequencies. This can be related to the geometrical distance between the error microphone and the control loudspeaker and the corresponding acoustic response, which means that small surge movements for error microphones close to the secondary loudspeakers can cause a relatively large increase in the magnitude of the response, which leads to a significant difference between the plant model and the physical plant response, leading to a significant degradation in performance. This behaviour is not observed in the case of forward surge due to the asymmetry in performance of the system as previously noted, which means that there is a decrease in the magnitude of the response in this case [25].

In the case of the narrow loudspeaker spacing configuration, which is shown in Fig. 9, the mismatch between the left and right microphones is less significant than for the wide loudspeaker spacing. For sway movements, as presented in Fig. 9(a), the frequency

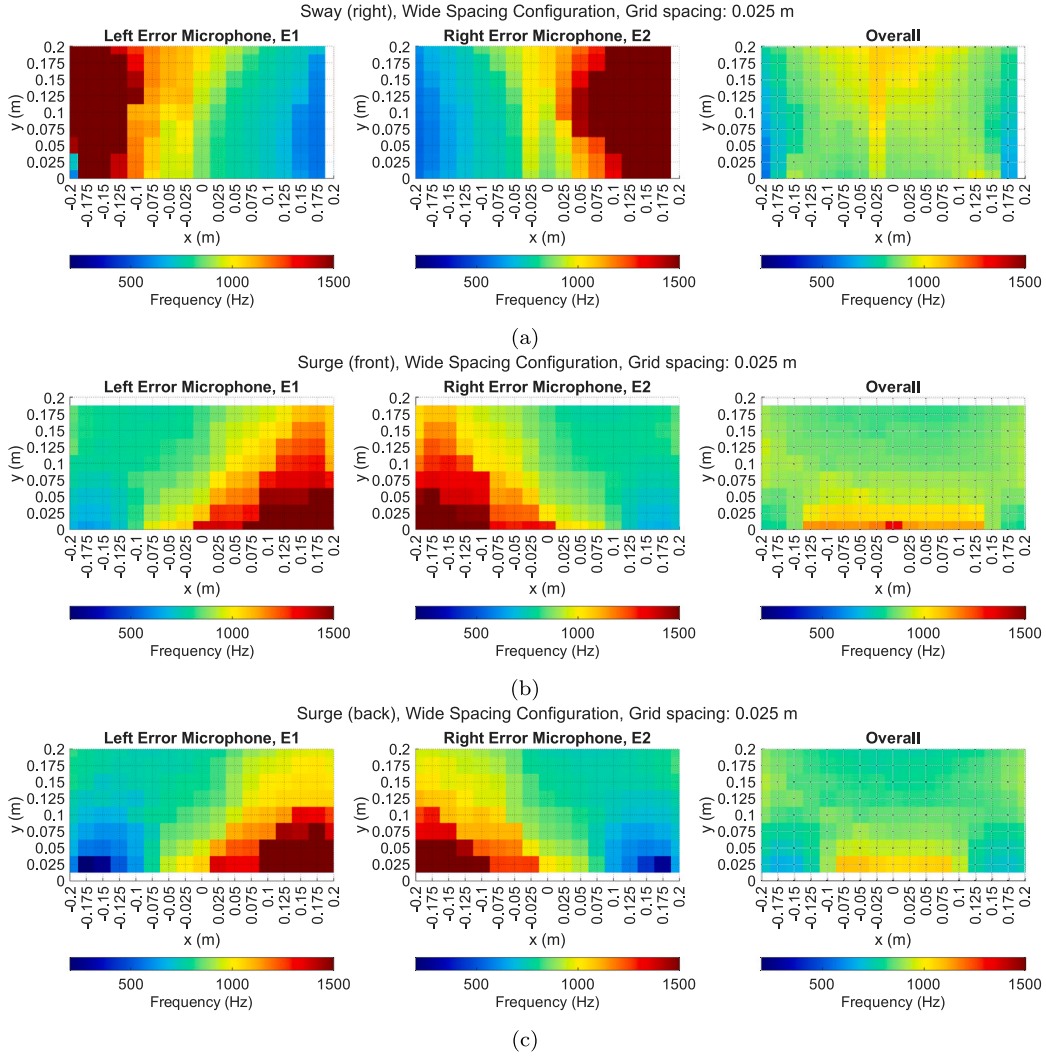

Fig. 8. The colour maps showing the frequency at which the attenuation level first crosses below 10 dB for (a): sway (right), (b): surge (front), (c): surge (back), mapped to the initial head positions for the wide spacing configuration. The unfilled regions represent initial head positions where head movement within the specified grid is infeasible.

at which the attenuation performance for the left and right error microphones first exceeds 10 dB is highest at $x = -0.05$ m and $x = 0.05$ m, respectively, and decreases in both the positive and negative x-directions. It can also be seen from these results that a prominent region occurs where the 10 dB crossing frequency drops below 200 Hz for both the left and right error microphones at around $x = \pm 0.175$ m, and this is consistent with the low percentage values observed in Fig. 7(b) for sway movements in the narrow loudspeaker configuration. Despite this, the differences between the left and right error microphones are clearly much smaller than in the wide loudspeaker spacing configuration. This is because, in the case of the narrow loudspeaker spacing, the changes in straight-line propagation distance are not only smaller but also more similar for the left and right direct paths, particularly around the central region. As a result, the overall performance is quite similar to that achieved at the individual microphones, with a central region of high performance and a reduced tracking range in the regions around $x = \pm 0.2$ m, which is consistent with the larger variation in overall attenuation performance observed for sway movements in Fig. 6(b). For forward and backward surge movements, as shown in Fig. 8(b) and Fig. 8(c), there is less variation in the 10 dB crossing frequency, with a value of around 800 Hz occurring across the majority of the tracking grid. While differences can still be observed at around (±0.2, 0) m, the region is considerably smaller than observed for the wide loudspeaker spacing configuration.

Fig. 10 presents a similar plot to Fig. 8 and Fig. 9, but for head rotation. For conciseness, only three initial head rotation angles are shown in three separate rows, corresponding to −27°, 0°, and +18°. The results indicate that the performance for both headrest configurations depends on the initial head rotation angle. In the wide spacing configuration, as shown in Fig. 10(a), the region where the 10 dB crossing frequency falls below 1 kHz is observed at $0.05 \leq x \leq 0.2$ m for both the left and right microphones for an

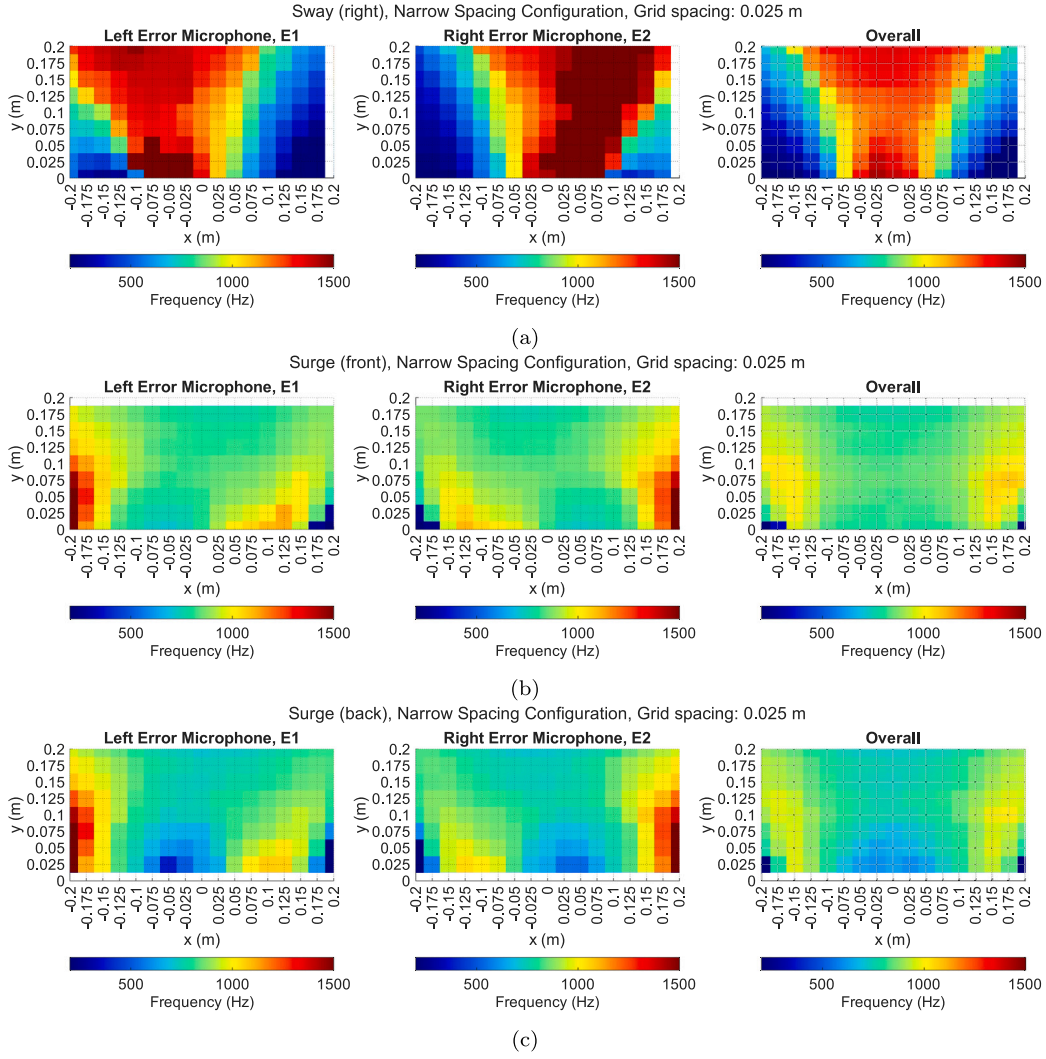

Fig. 9. The colour maps showing the frequency at which the attenuation level first crosses below 10 dB for (a): sway (right), (b): surge (front), (c): surge (back), mapped to the initial head positions for the narrow spacing configuration. The unfilled regions represent initial head positions where head movement within the specified grid is infeasible.

initial head rotation of −27°. For an initial head rotation of 0°, this region shifts to $-0.2 \leq x \leq -0.125$ m for the left microphone and $0.125 \leq x \leq 0.2$ m for the right microphone, highlighting a mismatch in behaviour between the left and right microphones. Finally, for an initial head rotation of +18°, the same region for both microphones shifts again to $-0.2 \leq x \leq -0.05$ m, showing a mirrored spatial symmetry compared to the −27° initial head rotation case. For the narrow spacing configuration, as shown in Fig. 10(b), a more pronounced difference is observed between the left and right error microphones. At an initial head rotation of −27°, the region where the 10 dB crossing frequency falls below 200 Hz is located at $0.125 \leq x \leq 0.2$ m for the left microphone, whereas, the 10 dB crossing frequency exceeds 1 kHz in this same region for the right microphone. A similar behaviour is observed at +18°, where the frequency exceeds 1 kHz for the left microphone for $-0.2 \leq x \leq -0.125$ m, while it falls below 200 Hz for the right microphone in this region. However, at 0°, the region where the frequency falls below 200 Hz appears at (0.2, 0) m and (−0.2, 0) m for the left and right microphones, respectively. It is interesting to observe the general differences in the performance between translational and rotational head movements for the wide and narrow spaced loudspeaker configurations. In particular, while the narrow loudspeaker spacing provides more uniform behaviour across the tracking grid for translational movements, it exhibits a more significant variation in performance for rotational movements.

The results presented above have demonstrated that a mismatch in the control bandwidth between the left and right error microphones occurs, however, they do not allow any mismatch in the achieved attenuation over frequency to be observed, which will be critical to the perceived performance of an active headrest system. To examine this aspect, Fig. 11 presents the attenuation performance as a function of frequency for two initial head positions undergoing sway movement for the two different

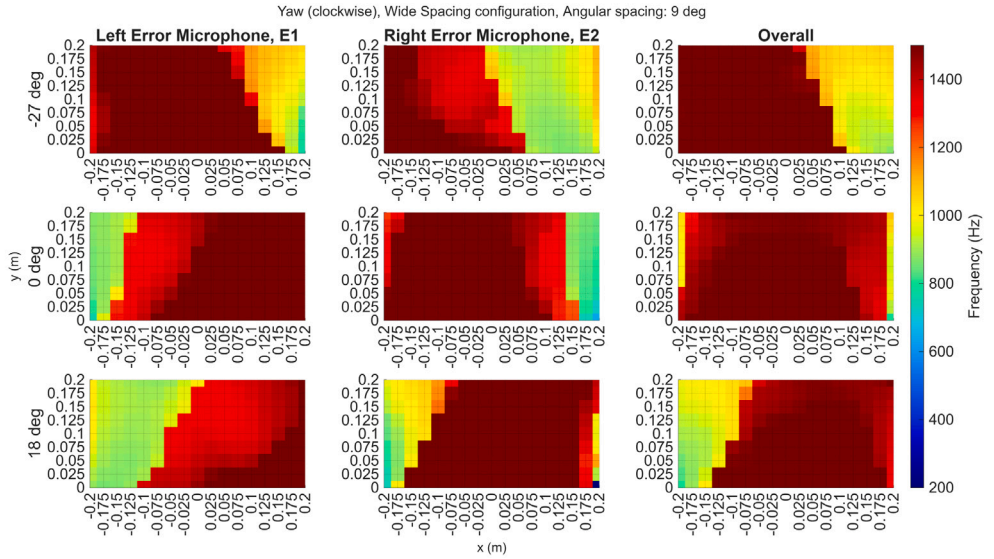

Fig. 10. The colour maps showing the frequency at which the attenuation level first crosses below 10 dB for the case of clockwise yaw rotation, mapped to the initial head positions and rotations for the (a): wide spacing and (b): narrow spacing configuration.

headrest loudspeaker configurations. The results reveal that the difference in attenuation performance between the individual microphones depends on both the initial head position and the headrest configuration. For example, for the wide loudspeaker spacing configuration, when the head is initially positioned at (0, 0.05) m and undergoes sway movement, as shown in Fig. 11(a) by the solid lines, similar attenuation performance is achieved at the left and right error microphones across the presented frequency range. In contrast, when the head is initially positioned at (0.1, 0.05) m, as depicted in Fig. 11(b), the attenuation performance at the right error microphone is consistently 7 dB higher than for the left microphone. This imbalance in noise attenuation between the left and right error microphones is due to the modelling errors that arise as a result of head movements, which depend on both the type of head movement and the initial head position. In the case of the narrow loudspeaker spacing configuration, represented by the dashed lines in both figures, a consistent 4 dB mismatch in attenuation performance between the left and right error microphones is observed for the initial head position of (0, 0.05) m, although the level of attenuation performance is consistently higher than for the wide loudspeaker spacing configuration. However, for the initial head position of (0.1, 0.05) m, the mismatch between the left

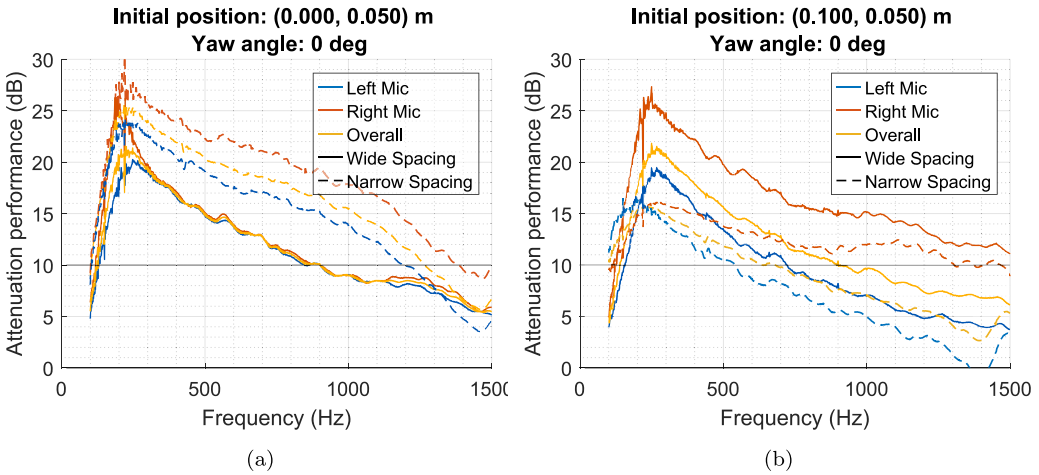

Fig. 11. The overall attenuation performance and attenuation performance at the individual error microphones for the two headrest configurations, shown for sway movement with a tracking resolution of 0.025 m, at initial head positions of (a): (0, 0.05) m and (b): (0.1, 0.05) m.

and right microphones increases with frequency, further emphasising the role of both the initial head position and the loudspeaker arrangement in determining the attenuation performance.

5. Conclusions

The performance of local active noise control headrest systems during head movements can be enhanced by incorporating head-tracking techniques. However, the benefits of head tracking may be constrained by various design factors, including the geometrical arrangement of the secondary loudspeakers and the tracking resolution used to predefine a finite set of plant responses within the tracking range. This paper has presented an investigation into how the tracking resolution and the geometrical configuration of the headrest loudspeakers affect the controller performance limitations, which provides new physical insight that can support the design methodology utilised in the realisation of local active noise control headrests with head-tracking.

The results presented in this paper are based on offline simulations using experimentally measured responses for various head positions and rotations within a defined tracking grid, and for two different headrest loudspeaker spacings. For the purposes of this fundamental study that aims to provide physical insight, it is assumed that the statistical properties related to the disturbance signals at the ears are known, a perfect reference signal is available, the controller is not causally constrained, and the nearest-neighbour method of updating the plant model is utilised. The effect of tracking resolution on the control performance is examined separately across three degree of freedom, that is sway and surge translational movements, and yaw rotation, and the influence that the headrest geometry has on the performance is also explored.

In the first instance the effect of loudspeaker spacing on the variation in the plant response across the tracking grid is investigated. This demonstrates that, while the narrower loudspeaker spacing exhibits larger variance in the magnitude response due to the proximity between the ears and the loudspeakers, the range of variation in the phase response remains relatively consistent between the two loudspeaker configurations. It is then demonstrated how increasing the tracking resolution increases the control performance, but interestingly, the overall performance averaged across all head movements is relatively insensitive to the loudspeaker spacing. More notably, however, it is observed that the narrow loudspeaker spacing in general shows a larger variation in the level of control performance across the tracking grid. In practical application, it is important that a head-tracked local active noise control system is able to maintain consistent performance across the tracking grid and, therefore, the spatial variance in control performance is investigated in more detail. In particular, it is shown that the wide loudspeaker spacing provides a more uniform overall performance across the tracking range, but can introduce a quite significant difference in performance between the two ears. Conversely, while the narrow loudspeaker spacing achieves a better balance in the attenuation achieved at the two ears, the spatial extent of the effective tracking range is reduced.

It is important to emphasise that the clear trends observed in this study are enabled by the assumed anechoic environment, which means that the performance degradation neglects any secondary effects that may occur in a practical reverberant environment. That said, the presented study provides a foundation for future work that includes similar investigations in realistic acoustic environments, where additional reflections from surrounding structures are present. The use of a constant regularisation parameter in this work also allows physical insights into the behaviour of the control system to be more clearly observed, however, for practical realisations it may be beneficial to optimally tune the regularisation parameter, as investigated in Ref. [17], and to potentially independently regularise each control signal to improve the balance in attenuation performance between the two ears. Furthermore, modelling errors associated with the primary disturbance, particularly those arising from virtual sensing techniques [8,26], should also be examined.

Finally, it should be noted that the trends observed in this study are sensitive to the chosen head-tracking range. For instance, if the tracking range were reduced – for example, by halving the dimension in the x-axis to give an area of 0.2 m × 0.2 m – the imbalance in attenuation performance between the two ears observed in the considered case with an area of 0.4 m × 0.2 m would be expected to reduce. Still, the observations made in this work have highlighted the interplay between the head-tracking resolution and the headrest loudspeaker arrangement and the associated performance trade-offs that need to be considered when designing a local headrest active noise control system with head-tracking.

CRediT authorship contribution statement

Chung Kwan Lai: Writing – original draft, Visualization, Validation, Methodology, Investigation, Formal analysis, Data curation. **Jordan Cheer:** Writing – review & editing, Supervision, Resources, Project administration, Methodology, Funding acquisition, Conceptualization.

Declaration of competing interest

The authors declare that they have no known competing financial interests or personal relationships that could have appeared to influence the work reported in this paper.

Acknowledgements

The work was supported by the project IN-NOVA: Active reduction of noise transmitted into and from enclosures through encapsulated structures, which has received funding from the European Union's Horizon Europe programme under the Marie Sklodowska-Curie grant agreement no. 101073037. This work was funded by UK Research and Innovation under the UK government's Horizon Europe funding guarantee [grant number EP/X027767/1]. Jordan Cheer was supported by the Department of Science, Innovation and Technology (DSIT) Royal Academy of Engineering under the Research Chairs and Senior Research Fellowships programme.

Data availability

Data will be made available on request.

References

[1] P.A. Nelson, S.J. Elliott, Active Control of Sound, Academic Press, 1992.
[2] H.F. Olson, E.G. May, Electronic sound absorber, J. Acoust. Soc. Am. 25 (6) (1953) 1130–1136, http://dx.doi.org/10.1121/1.1907249.
[3] B. Rafaely, S.J. Elliott, J. Garcia-Bonito, Broadband performance of an active headrest, J. Acoust. Soc. Am. 106 (2) (1999) 787–793, http://dx.doi.org/10.1121/1.427134.
[4] P.A. Nelson, A.R.D. Curtis, S.J. Elliott, A. Bullmore, The active minimization of harmonic enclosed sound fields, part I: Theory, J. Sound Vib. 117 (1987) 1–13, http://dx.doi.org/10.1016/0022-460X(87)90432-9.
[5] S.J. Elliott, P. Joseph, A.J. Bullmore, P.A. Nelson, Active cancellation at a point in a pure tone diffuse sound field, J. Sound Vib. 120 (1) (1988) 183–189, http://dx.doi.org/10.1016/0022-460X(88)90343-4.
[6] A. Roure, A. Albarrazin, The remote microphone technique for active noise control, in: Active99, Fort Lauderdale FL, USA, 1999, pp. 1233–1244.
[7] M. Pawelczyk, Adaptive noise control algorithms for active headrest system, Control Eng. Pract. 12 (9) (2004) 1101–1112, http://dx.doi.org/10.1016/j.conengprac.2003.11.006.
[8] D. Moreau, B. Cazzolato, A. Zander, C. Petersen, A review of virtual sensing algorithms for active noise control, Algorithms 1 (2) (2008) 69–99, http://dx.doi.org/10.3390/a1020069.
[9] J. García-Bonito, S. Elliott, Active cancellation of acoustic pressure and particle velocity in the near field of a source, J. Sound Vib. 221 (1) (1999) 85–116, http://dx.doi.org/10.1006/jsvi.1998.1989.
[10] C. Lei, J. Xu, J. Wang, C. Zheng, X. Li, Active headrest with robust performance against head movement, J. Low Freq. Noise Vib. Act. Control. 34 (3) (2015) 233–250, http://dx.doi.org/10.1260/0263-0923.34.3.233.
[11] S.J. Elliott, W. Jung, J. Cheer, Head tracking extends local active control of broadband sound to higher frequencies, Sci. Rep. 8 (1) (2018) 1–7, http://dx.doi.org/10.1038/s41598-018-23531-y.
[12] Y. Liu, H. Li, H. Zou, Z. Lin, J. Lu, Active headrest combined with a depth camera-based ear-positioning system, J. Acoust. Soc. Am. 157 (1) (2025) 519–526, http://dx.doi.org/10.1121/10.0034860.
[13] W. Jung, S.J. Elliott, J. Cheer, Local active control of road noise inside a vehicle, Mech. Syst. Signal Process. 121 (2019) 144–157, http://dx.doi.org/10.1016/j.ymssp.2018.11.003.
[14] L. Yang, L. Zhang, H. Dong, A. Alelaiwi, A. El Saddik, Evaluating and improving the depth accuracy of kinect for windows v2, IEEE Sensors J. 15 (8) (2015) 4275–4285, http://dx.doi.org/10.1109/JSEN.2015.2416651.
[15] H. Su, J. Liu, A. Liu, B. Li, A study of an active noise control system with continuous tracking of the human ear and noise segmentation control, Int. J. Automot. Technol. (2025) http://dx.doi.org/10.1007/s12239-024-00207-3.
[16] J.Y. Oh, H.W. Jung, M.H. Lee, K.H. Lee, Y.J. Kang, Enhancing active noise control of road noise using deep neural network to update secondary path estimate in real time, Mech. Syst. Signal Process. 206 (2024) 110940, http://dx.doi.org/10.1016/j.ymssp.2023.110940.
[17] F. Veronesi, C.K. Lai, J. Cheer, Interpolation between plant responses in a head-tracked local active noise control headrest system, Mech. Syst. Signal Process. 240 (2025) 113401, http://dx.doi.org/10.1016/j.ymssp.2025.113401.
[18] S. Elliott, Signal Processing for Active Control, Academic Press, 2000.
[19] C.K. Lai, J. Cheer, C. Shi, The effect of head-tracking resolution on the stability and performance of a local active noise control headrest system, J. Acoust. Soc. Am. 157 (2) (2025) 766–777, http://dx.doi.org/10.1121/10.0035576.

[20] C.K. Lai, J. Cheer, Parametric study of loudspeaker spacing in an active noise control headrest system with head-tracking, in: 54th International Congress & Exposition on Noise Control Engineering, Sao Paulo, Brazil, 2025.
[21] S.J. Elliott, J. Cheer, Modeling local active sound control with remote sensors in spatially random pressure fields, J. Acoust. Soc. Am. 137 (4) (2015) 1936–1946, http://dx.doi.org/10.1121/1.4916274.
[22] H. Jiang, H. Chen, J. Tao, H. Zou, X. Qiu, Accuracy requirements of ear-positioning for active control of road noise in a car, Appl. Acoust. 225 (2024) 110164, http://dx.doi.org/10.1016/j.apacoust.2024.110164.
[23] A. Farina, Simultaneous measurement of impulse response and distortion with a swept-sine technique, J. Audio Eng. Soc. 48 (2000) 419–444.
[24] D.S. Brungart, W.M. Rabinowitz, Auditory localization of nearby sources. Head-related transfer functions, J. Acoust. Soc. Am. 106 (3) (1999) 1465–1479, http://dx.doi.org/10.1121/1.427180.
[25] G.A. Mangiante, Active sound absorption, J. Acoust. Soc. Am. 61 (6) (1977) 1516–1523, http://dx.doi.org/10.1121/1.381453.
[26] W. Jung, S.J. Elliott, J. Cheer, Combining the remote microphone technique with head-tracking for local active sound control, J. Acoust. Soc. Am. 142 (1) (2017) 298–307, http://dx.doi.org/10.1121/1.4994292.